



3D NUMERICAL ANALYSIS OF COMPOSITE PILED RAFT FOUNDATION ON SOFT CLAY

Received: 28-03-2025

Accepted: 08-04-2025

Ahmed M. Abdel Galil ^a, Mohamed I. Elsalty ^{b,c,*}, Abdel-Fattah A. Youssef ^a

^a Civil Engineering Department, Faculty of Engineering, Menoufia University, Menoufia, Egypt.

^b Ph.D. Candidate, Civil Engineering Department, Faculty of Engineering, Menoufia University, Menoufia, Egypt.

^c Civil Engineering Department, Higher Institute of Engineering and Technology in Kafr El sheikh, Egypt.

* Corresponding author: M. I. Elsalty (mohamed.elsalty@kfs-hiet.edu.eg)

ABSTRACT. Building on soft clay, commonly found in many regions of Egypt, often encounters challenges such as excessive settlement and bearing capacity failures. The composite piled raft foundation (CPRF) is a recently developed foundation system that offers an economical substitute for traditional piled rafts for medium-rise buildings on soft clay. In the CPRF, two types of disconnected piles, differing in stiffness and length, are used to strengthen the soft clay and reduce foundation settlement. A deformable cushion separates the piles from the raft to adjust the load sharing between the piles and the subsoil. This study investigates the performance of uniformly loaded CPRF on soft clay in drained conditions. Three-dimensional finite element analyses are performed to evaluate the influence of various factors, including the area replacement ratio, the length and stiffness of short piles, and the thickness and stiffness of the cushion on the performance of the CPRF. The impact of these parameters is evaluated based on the settlement behavior of the CPRF, the load shared by the long piles, short piles, and the subsoil, as well as the axial loads experienced by the long piles. The numerical results reveal the presence of optimal values among the studied factors. The outcomes of this study could be used as a basis for achieving economical design of the CPRF resting on soft clay.

KEYWORDS: Composite piled raft foundation; Soft clay; Disconnected piles; Area replacement ratio; Short piles

1. INTRODUCTION

Foundations are constructed to safely and economically transmit the structure's load to the underlying soil, assuring the structure's stability and serviceability. Shallow foundations like rafts are suitable foundations when a soil stratum having sufficient bearing capacity and settlement characteristics is present at relatively shallow depths. However, when raft foundations do not satisfy the design requirements, deep foundations are employed to transfer the applied loads to deeper bearing layers.

Piled raft (PR) foundations are considered an effective solution for high-rise buildings. This sort of foundation is composed of three key elements: subsoil, raft, and piles. These elements interact in a complicated way, which includes interactions between piles and soil, piles and raft, and raft and soil. In PRs, the piles and the raft both

contribute to transferring the applied loads from the superstructure to the soil, in contrast to traditional pile foundations, where the piles alone are assumed to bear the entire load, disregarding the load-bearing contribution of the raft [1-5].

The utilization of piles in PR foundations as settlement reducers optimized the design by significantly reducing the number of piles required [6-8]. However, structurally connecting these fewer piles to the raft can lead to excessive bending moments and concentrated axial stresses at the tops of the piles [9-10]. To resolve these problems, a new foundation system called the disconnected piled raft (DPR) is proposed by [11]. This system involves the placement of a layer of compacted granular material (i.e., a cushion) to uniformly redistribute and adjust the stress distribution between the piles and the underlying soil. The disconnected settlement-reducing piles in this system do not act as structural elements but instead function as reinforcement for

the underlying soil, enhancing its overall behavior [12-20].

In PR foundations, the raft's load-carrying capacity is mainly affected by the bearing interaction between the raft and the topsoil. This interaction becomes notable when soil profiles at shallow depths are composed of dense sand or stiff clay. However, in situations where the soil profile contains soft clays near the surface, the soft soil's low bearing strength and high compressibility result in inadequate raft-soil bearing interaction, reducing the raft's contribution to the overall piled raft foundation [21-22]. To effectively improve the raft-soil interaction and, consequently, enhance the raft's loading capacity, Liang et al. [23] developed a new type of disconnected piled raft foundation known as the composite piled raft foundation (CPRF), or long-short composite piled raft foundation with an intermediate cushion.

The components of the CPRF include: (1) long piles formed of stiff materials, functioning as either floating or end bearing, which are used to minimize raft settlement; (2) short piles of relatively flexible materials that are employed to enhance the carrying capacity of shallow soft soil; (3) a granular cushion layer composed of compacted coarse-grained soil, placed among the raft and piles, is used to optimize the stress distribution between the piles and subsoil; and (4) a reinforced concrete raft that transmits loads of the structure into the subsoil.

Several numerical and experimental research have been performed recently to investigate the behavior of both CPRF and DPR foundations since the invention of these new foundation systems.

Liang et al. [23] examined the behavior of CPRF using 3D FEM analysis with ANSYS software, finding that the cushion layer assists in distributing load-sharing ratios among the piles, improving the utilization of the short piles' bearing capacities and enhancing the efficiency of the shallow subsoil's bearing capacity.

Zhao et al. [24] completed a detailed study on the mechanical behavior of CPRF. In their research, they carefully considered the influence of the cushion and assessed the flexibility of the various components involved in the interaction within the foundation system. Based on their analysis, they proposed a method for calculating the settlement of the CPRF.

Zheng et al. [25] used 3D numerical analysis to investigate a CPRF system that included lime-treated short piles, cement-fly ash-gravel (CFG) long piles, a

sand cushion, and a raft. They found that the settlement is significantly influenced by the diameter and length of the CFG long piles, whereas the lime short piles have a lesser impact. Additionally, the thickness of the cushion plays a key role in distributing loads among the piles and the subsoil.

Wang et al. [26] planned and performed laboratory experiments on multi-element composite foundations with various combinations of vertical short and long piles. The findings indicated that multi-element composite foundations, like those combining steel pipe long piles with sand short piles or concrete long piles with lime short piles, have a better load carrying capacity than composite foundations made entirely of sand short piles under identical circumstances.

Eslami and Malekshah [27] conducted three-dimensional finite element analysis of the DPR foundation with ABAQUS program. Based on the findings, the highest axial stress across the piles occurred at varying depths, based on the cushion's stiffness and thickness.

Moayed et al. [28] used ABAQUS program to examine the influence of various factors, like raft thickness, long pile length, and short pile modulus, on the behavior of the CPRF, while Sharma et al. [29] explored the same using MIDAS GTS program.

El Kamash et al. [30] used ABAQUS software to study the efficiency of the DPR foundation in various soft clays using several pile materials such as sand columns, stone columns, and concrete columns. They also examined the impact of design characteristics, including pile spacing, embedment length, and configuration, as well as the granular layer's thickness and stiffness, and raft thickness, on the DPR foundation's behavior.

El-Garhy [31] used a simplified plate-on-springs methodology to examine the impact of several parameters on the behavior of the CPRF, such as the number of short and long piles, the short piles' area ratio, as well as the rigidity of both the short piles and the cushion.

The existing literature reveals the challenges associated with the performance of the CPRF in soft clay due to the complex interactions among the raft, cushion, soft soil, long piles, and short piles. Further research is needed to fully comprehend these complex interactions, ensuring the creation of a reliable design and the appropriate use of CPRF in engineering applications.

The main goal of this study is to develop a deeper understanding of the performance of CPRF on soft clay under uniform loads in drained conditions. The complex soil-structure interactions are investigated through three-dimensional finite element analyses using PLAXIS 3D V2020 software [32]. A parametric study is carried out to assess the effect of the area replacement ratio, length and stiffness of short piles, and the stiffness and thickness of the cushion on CPRF performance. The impact of these parameters is analyzed based on the settlement performance of the CPRF, the load-sharing ratios of the short piles, long piles, and the subsoil, as well as the axial loads on long piles.

2. NUMERICAL MODELING

2.1. PROBLEM DEFINITION

This research investigates the performance of CPRF resting on a soil profile composed of a top layer of soft clay with a thickness of 16 m, underlain by a large extended layer of dense sand. The groundwater level is assumed to be at the bottom of the cushion layer. Fig. 1. presents a schematic representation of the studied CPRF, which consists of a 16.0 m × 16.0 m rigid square raft with a thickness of 1.0 m. The raft is supported by two types of disconnected piles, varying in stiffness and length, which are uniformly distributed beneath the raft in a square pattern. The first type consists of 36 long concrete end-bearing piles, each with a diameter (D_{Lp}) of 0.40 m and a length (L_{Lp}) of 17.0 m, arranged with constant spacing of $7 D_{Lp}$ (i.e., 2.80 m). The second type includes 85 short flexible floating piles, positioned between the long piles at constant spacing of $3.5 D_{Lp}$ (i.e., 1.40 m) from the adjacent pile. The length (L_{sp}), diameter (D_{sp}), and stiffness of short piles are varied through the analyses. A cushion layer, with a variable thickness (t_c) and stiffness, is placed between the raft and the disconnected piles.

Disconnected long and short piles are employed to improve the soft clay under the raft to achieve the required serviceability and shear strength criteria. The presence of these piles could be represented by their area ratios relative to the raft. The area ratio of the long piles (A_{rlp}) is the ratio of the total area of the long piles to the area of the raft. Similarly, the area ratio of the short piles (A_{rsp}) is the ratio of the total area of the short piles to the area of the raft. The total area ratio (A_r) is the sum of the area ratios of both pile types.

In the present study, the A_{rsp} is adjusted by

varying the diameter of the short piles, while the A_{rlp} is kept constant.

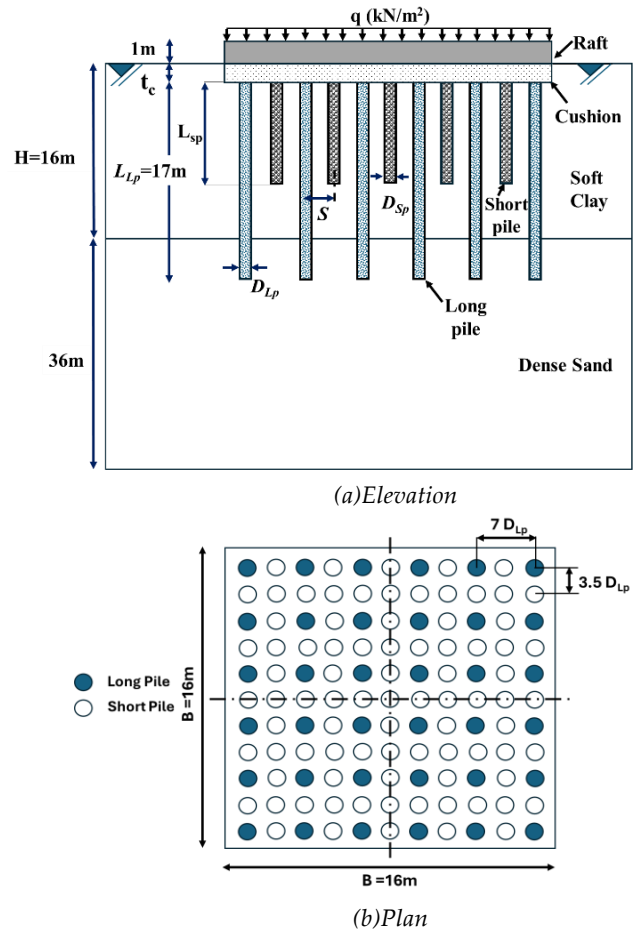


Fig. 1. Schematic representation of the CPRF analyzed in the current research.

2.2. FINITE ELEMENT MODEL

A 3D FE model is created to simulate the studied uniformly loaded CPRF resting on soft clay using PLAXIS 3D software. Since the analyzed CPRF is symmetrical about the X and Y axes, only a quarter of the foundation system is modeled, as depicted in Fig. 2, to reduce the model size and thereby save computational time.

The model boundaries are chosen so that they have no effect on the foundation's performance. The bottom boundary is set at a distance three times the length of the long pile measured from the pile head and is fixed against movements in both vertical and horizontal directions. While the lateral surrounding boundaries of the model are set at a distance five times the raft width, measured from the raft centerline. These boundaries are constrained horizontally but are permitted to move vertically.

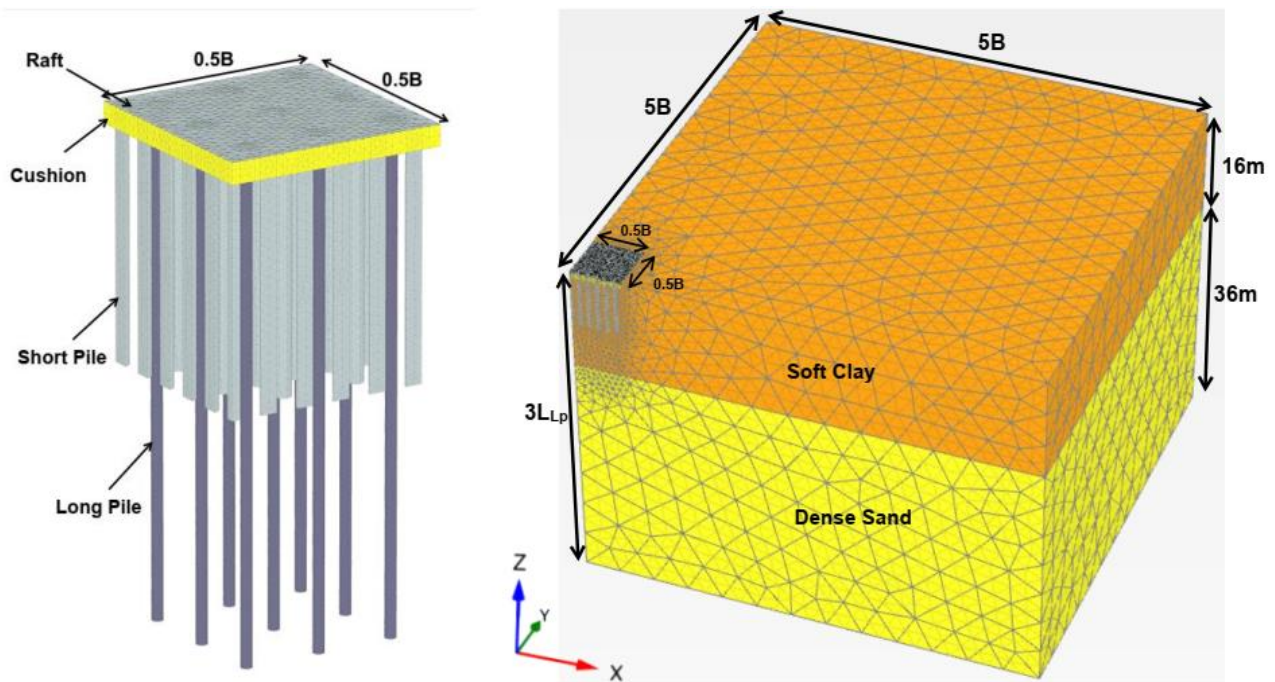


Fig. 2. The FE model utilized in the present study.

A medium meshing scheme is used for the entire model, with local refinement applied to the region close to the raft-cushion-piles system, which is exposed to large stress concentrations and significant deformations, to enhance the accuracy of the results.

The Hardening Soil (HS) model is used to model the geotechnical elements, including the subsoil (comprising soft clay and dense sand layers), cushion layer, and short flexible piles. The HS model is a sophisticated approach for simulating the nonlinear behavior of the soil offering a more accurate representation of soil stiffness by incorporating key parameters such as triaxial secant stiffness (E_{50}), oedometer tangent stiffness (E_{oed}), and unloading-reloading stiffness (E_{ur}) [33]. The properties of the soft clay are selected according to the findings of El-Nahas et al. [34], while the characteristics of the sand (both within the soil profile and as cushion material) are derived from the correlation established by [35] based on the relative density (D_r). The material properties of the flexible piles are obtained from the research conducted by [36]. The analysis of the geotechnical materials is conducted under drained conditions.

In contrast, the Linear Elastic (LE) model is used to model the raft and concrete long piles, based on the assumption that their significantly higher elastic moduli, compared to the surrounding soil, keep them within an elastic state.

In this analysis, the long and short piles are

represented as volume elements, whereas the raft is represented as a plate element. Table 1 provides the properties of the subsoil, piles, and raft used in the present numerical model.

Interface elements, assumed to have zero thickness, are employed to represent the interaction of soil and structural components. The shear strength of these elements is defined by the interface reduction factor (R_{inter}). The R_{inter} is assigned values of 0.85, 0.67, and 1 for the soft clay layer, sandy soil, and short piles, respectively [34].

The CPRF construction process is represented in several phases. In the initial phase, the soil domain is activated to generate the geostatic stresses. During the second phase, the construction of long and short piles, cushion, interfaces, and raft is simulated. In the final phase, the load is applied to the raft.

2.3. MODEL VALIDATION

To confirm the reliability and accuracy of the current FE analysis, the numerical model used in this study is validated using the experimental results obtained by Wang et al. [26]. They performed laboratory experiments on multi-element composite foundations, using various combinations of long and short piles. For validation, the specific case of CPRF, which combines steel pipe long piles and sand short piles, is selected as it exhibited the least settlement compared to the other cases.

In the selected CPRF experimental model, a steel raft with a thickness of 30 mm and dimensions of 500 mm × 500 mm is used, with a 50 mm thick coarse sand cushion placed beneath it. The raft is reinforced by a single steel long pile located at the center, along with four short sand piles arranged in a 2 × 2 square pattern beneath the raft. The long pile has a diameter of 40.0 mm and a length of 400 mm, while each short pile has a diameter of 40.0 mm, and a length of 300 mm. Additional details of the experimental test are available in Ref. [26]. An FE

analysis is conducted using PLAXIS 3D, replicating the same experimental test conditions. The material characteristics utilized in the FE analysis are summarized in Table 2.

Fig. 3 compares the load-settlement curves obtained from the current FE analysis, the experimental study, and the numerical validation performed by Moayed et al. using ABAQUS [28]. As depicted in Fig. 3, the findings from the present FE analysis are in good agreement with those obtained in the experimental study and the ABAQUS analysis.

Table 1. Materials properties utilized in the FE analysis.

Material	Subsoil		Cushion (Dense sand)	Piles		Raft (RC)	Units
	Soft clay	Dense sand		Long Piles (PC)	Short Piles (SC)		
Model	HS	HS	HS	LE	HS	LE	-
Drainage type	Drained	Drained	Drained	Non-Porous	Drained	Non-Porous	-
γ_{sat}	16	18	18	22	19	25	kN/m ³
γ_{unsat}	16	18	18	-	19	-	kN/m ³
ν	0.3	0.2	0.2	0.15	0.3	0.15	
C	1	0	0	-	1	-	kN/m ²
ϕ	22	38	38	-	45	-	Degree
ψ	0	8	8	-	15	-	Degree
E	-	-	-	22e ⁺⁶	-	22e ⁺⁶	kN/m ²
E_{50}^{ref}	3120	48000	48000	-	70000	-	kN/m ²
E_{oed}^{ref}	2100	48000	48000	-	70000	-	kN/m ²
E_{ur}^{ref}	9360	144000	144000	-	210000	-	kN/m ²
R_{inter}	0.85	0.67	0.67	-	1	-	

Note: PC: Plain Concrete, SC: Stone Column, RC: Reinforced Concrete

Table 2. Materials properties utilized in the validation.

Parameter	Subsoil (Soft soil)	Cushion	Sand column	Steel (plate & pile)	Units
Model	HS	HS	HS	LE	-
Drainage type	Drained	Drained	Drained	Non-Porous	-
γ_{sat}	19.18	21.2	21.2	78.50	kN/m ³
γ_{unsat}	19.18	21.2	21.2	-	kN/m ³
ν	0.3	0.3	0.3	0.3	-
C	20	1	1	-	kN/m ²
ϕ	28	40	40	-	Degree
ψ	0	10	10	-	Degree
E	-	-	-	210e ⁺⁶	kN/m ²
E_{50}^{ref}	23400	60000	60000	-	kN/m ²
E_{oed}^{ref}	23400	60000	60000	-	kN/m ²
E_{ur}^{ref}	70200	180000	180000	-	kN/m ²

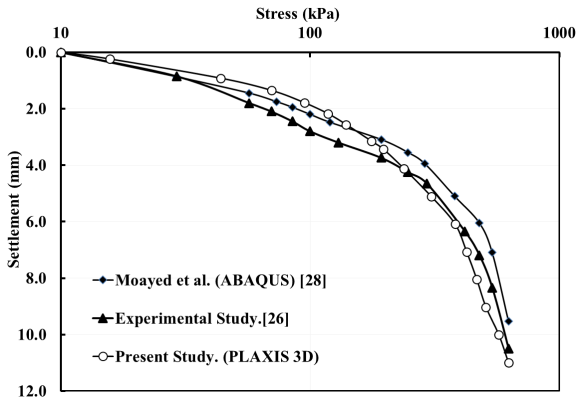


Fig. 3. Comparison of load-settlement curves of the current study, the experimental study [26], and the study by Moayed et al. using ABAQUS [28].

3. PARAMETRIC STUDY

3D FE analyses are employed to study the behavior of CPRF resting on soft clay under uniform loads in drained conditions. The numerical simulations are conducted under a uniform load of 100 kPa, representing the working load of a medium-sized building with approximately six stories.

The primary objective of the current parametric study is to evaluate the impact of the short piles' area replacement ratio, length, and stiffness, as well as the cushion's thickness and stiffness, on the load-carrying capacity of the CPRF. The study also investigates the load distribution between the long piles, short piles, and subsoil, in addition to the axial forces acting on the long piles.

In the parametric analysis, each parameter is altered individually while keeping all other parameters fixed at their reference values. Table 3 lists the parameters examined in this study, along with their corresponding values.

Table 3. Parameters and their values considered in the parametric study.

Parameter	Unit	Range of Values
Area ratio of the short piles, A_{rsp} (%)	-	4.2, 6.5, 9.3*, 16.7, 26.1
Length of the short piles, L_{sp}	m	3.20, 4.80, 6.40, 8*, 9.60, 16
Stiffness of the short piles, E_{sp}	MPa	38, 70*, 120, 320
Thickness of the cushion, t_c	m	0.25, 0.5, 0.75*, 1.0, 1.25, 1.50
Stiffness of the cushion, E_c	MPa	18, 30, 48*, 120

* Values of the reference case.

4. RESULTS AND DISCUSSION

4.1. GENERAL SETTLEMENT CHARACTERISTICS OF CPRF

To assess the impact of placing disconnected long and short piles under the raft on its settlement, the vertical settlement contours for the unpiled raft (without piles and cushion), DPR, and the reference case of CPRF, derived from the FE analyses under the same uniform vertical load of 100 kPa, are presented in Fig. 4.

For the unpiled raft, Fig. 4a demonstrates that the unpiled raft undergoes a maximum settlement of 563 mm, which greatly exceeds the permissible foundation settlement (i.e., 150 mm) according to [37]. This highlights the need for piles to decrease the raft's excessive settlement to a tolerable level. In the case of DPR, Fig. 4b illustrates that the presence of a limited number of disconnected rigid long piles under the raft reduces raft settlement to 182 mm. However, this settlement still surpasses the allowable foundation settlement. Furthermore, the target settlement criteria are satisfied by placing short flexible piles between the long rigid piles. As shown in Fig. 4c, the raft settlement is successfully reduced to 127.7 mm.

Since the settlement of the vertically loaded CPRF is strongly dependent on the settlements of the piles, the vertical settlements of both short and long piles are analyzed to enhance the understanding of the pile settlement mechanism. The results of the FE analyses, in terms of the vertical settlement profiles for the axes of the short and long piles near the raft center, along with the surrounding soil, are presented in Fig. 5 for the reference case of CPRF.

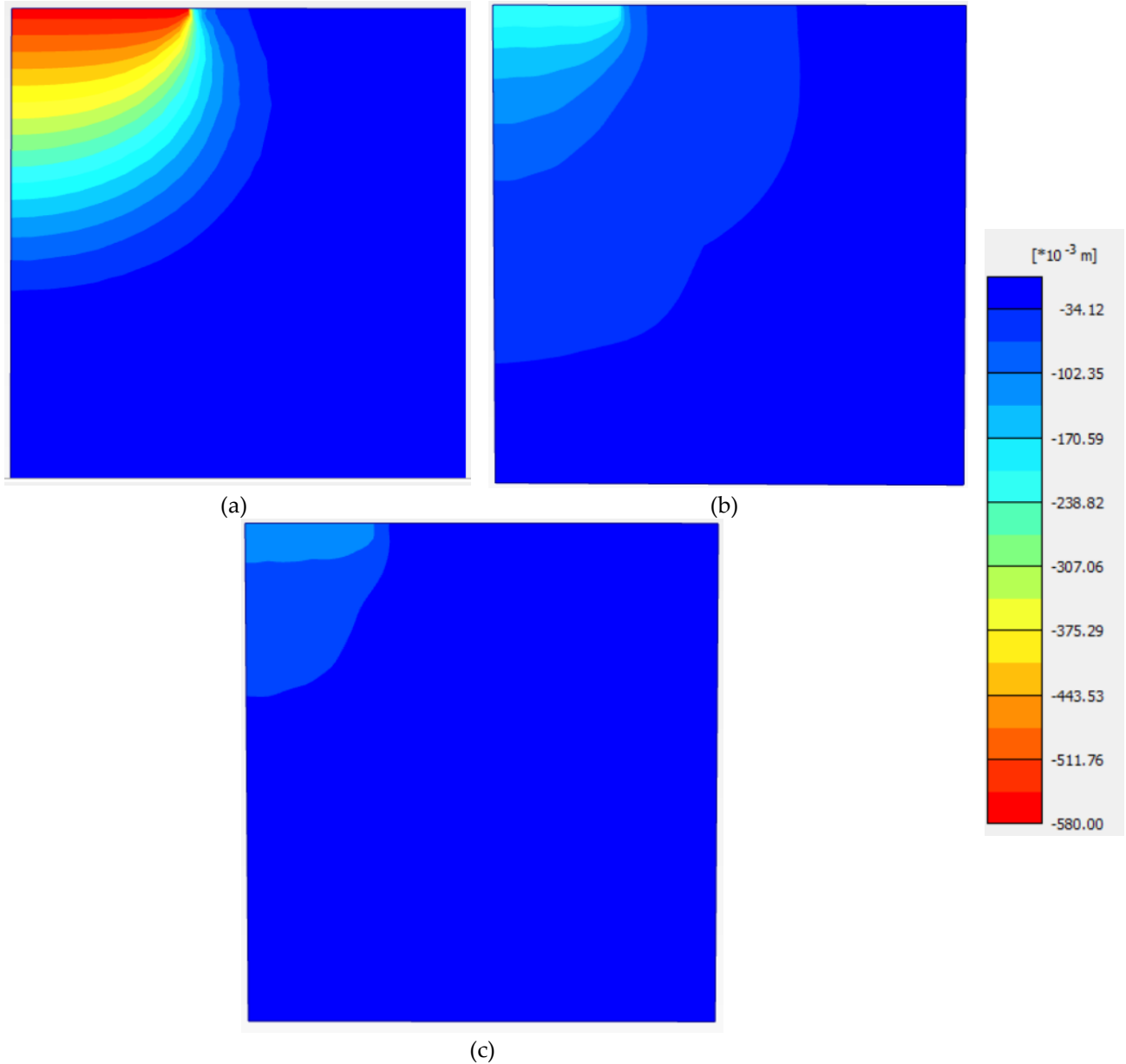


Fig. 4. Vertical settlement contours for: (a) UR, (b) DPR, (c) CPRF (the reference case).

The performance of the CPRF is significantly influenced by the presence of the granular cushion, which diminishes pressure concentration at the tops of long piles. Thereby, the load supported by the long piles is significantly reduced, while the shallow subsoil reinforced by the short piles supports a greater load. Consequently, the settlement of the subsoil is greater than that of both the short and long piles at the upper depths, as shown in Fig. 5. For instance, at the pile head, the settlements are 128.9 mm for the subsoil, 126.6 mm for the short pile, and 64.0 mm for the long pile.

Negative skin friction is mobilized along the upper pile shaft of both long and short piles due to the relative movement among the piles and the adjacent subsoil. With increasing depth, the

settlement of the subsoil progressively decreases until it matches the short pile's settlement at the location of its neutral plane.

At deeper levels, the settlement of the long pile equals the subsoil settlement, denoting the position of the long pile's neutral plane. Below the neutral plane, the subsoil settlement becomes smaller than the pile settlement, causing the transfer of load from the pile to the neighboring soil via friction along the pile's surface. Consequently, in the CPRF, the axial load on both short and long piles initially increases with depth, peaks at the neutral plane, and then decreases with further depth toward the pile tip. These findings align with those presented in [23].

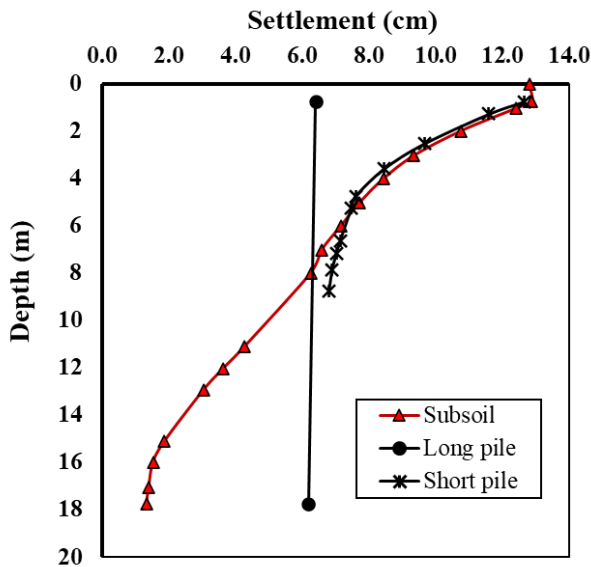


Fig. 5. Piles and subsoil settlement profiles of CPRF (the reference case).

4.2. EFFECT OF THE AREA RATIO OF THE SHORT PILES ON CPRF

The area ratio of the short piles (A_{rsp}) is varied within the range of 4.2% to 26.1% to investigate its impact on the performance of the CPRF. The various values of A_{rsp} are determined by varying the diameter of the short piles.

4.2.1. SETTLEMENT OF THE RAFT

Fig. 6 depicts the load-settlement curves of the DPR (with $A_{rsp} = 0$), and CPRF with various A_{rsp} ratios, applied with a uniform vertical load of 100 kPa. For all cases, the settlement was measured at the center of the raft. The data show that increasing the A_{rsp} reduces the settlement of the CPRF. This is due to the higher A_{rsp} , which indicates that a larger portion of the soft clay is replaced by the stiffer short pile material, enhancing the strength and stiffness of the shallow subsoil and improving the settlement behavior of the CPRF. This behavior aligns with the observations presented in [31]. However, it should be noted that the peak settlement surpasses the permissible values for the DPR system and CPRF with an A_{rsp} of 4.2%.

The benefit of using short piles with various A_{rsp} values to reduce the settlement of CPRF can be evaluated using a dimensionless parameter called the settlement reduction factor (SRF), which is identified to be the ratio between the settlement of the raft with both short and long piles (i.e., CPRF) to that of the raft with long rigid piles only (i.e., DPR) at the same load level.

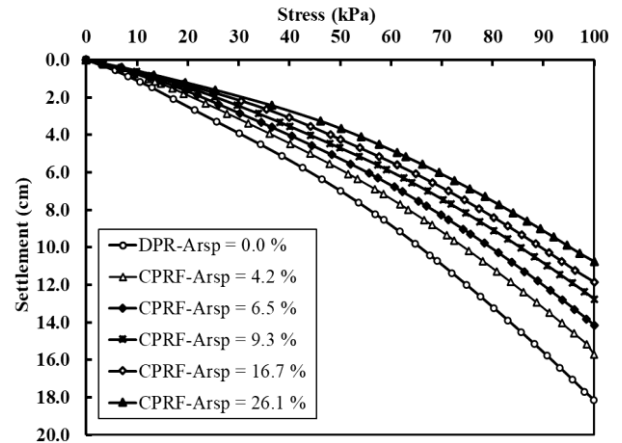


Fig. 6. Load-settlement curves for DPR and CPRF with different area ratio of short piles.

Fig. 7 illustrates the influence of the A_{rsp} on the SRF at a load level of 100 kPa. As depicted in Fig. 7, the SRF decreases with an increase in the area ratio of the short piles. When the A_{rsp} increases from 0% to 9.3%, the SRF decreases by about 29.8%. With further increases in the A_{rsp} , from 9.3% to 26.1%, the SRF continues to decrease but at a slower rate, with a reduction of only 16%. Therefore, with respect to the foundation settlement, the optimal A_{rsp} for the analyzed cases can be selected as 9.3%.

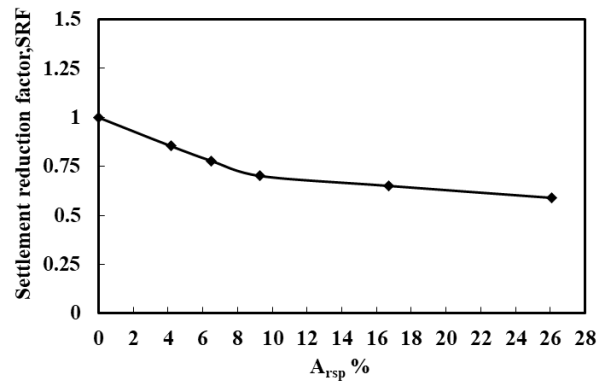


Fig. 7. Variation of settlement reduction factor with the area ratio of short piles at a load level of 100 kPa.

4.2.2. LOAD SHARING BETWEEN PILES AND SUBSOIL

In CPRF, the entire imposed load is distributed among the long piles, short piles, and subsoil among piles. The load carried by each of these components is often represented as a proportion of the entire induced load on the CPRF. From FE analysis results, the load borne by the long piles is obtained by dividing the total long pile head loads by the entire imposed load, while the load supported by the short piles is computed by dividing the total short pile top loads by the entire imposed load. Then, the load

supported by the subsoil is found by deducting the sum load shared by both long and short piles from 100.

Fig. 8 presents the effect of the A_{rsp} on the load borne by long piles, short piles, and the subsoil. As the A_{rsp} increases, the load shared by the short piles increases, while the load shared by both the subsoil and the long piles decreases. This is because increasing the A_{rsp} indicates that there is a greater replacement of the soft clay with the short pile's stronger material. This improves the strength and rigidity of the topsoil, resulting in transferring more load to the short piles and improving the bearing contribution of the raft. This behavior matches the results described in [22].

As the A_{rsp} increases from 0% to 26.1%, the short piles carry 28.3% of the entire load, while the load transmitted to the subsoil and the long piles decrease by 28.1% and 28.3%, respectively.

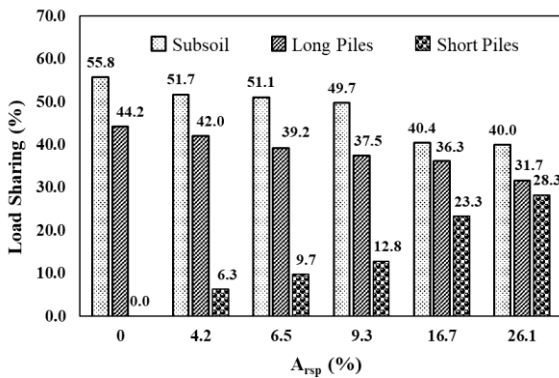


Fig. 8. Load sharing of CPRF for different area ratios of short piles at a load level of 100 kPa.

4.2.3. AXIAL LOAD ALONG THE LONG PILE

The impact of the A_{rsp} on the axial load through the long pile's length (near the raft center) within the CPRF is depicted in Fig. 9. The findings display that, regardless of the A_{rsp} value for the CPRF, the axial force in the disconnected long pile initially increases to its peak at the neutral plane and then gradually reduces. This behavior results from the formation of negative skin friction over the neutral plane through the pile surface. This pattern aligns with the settlement profiles of the soil and piles presented in Fig. 5.

Moreover, it is noted that the pile head axial load (N_{head}) and the maximum axial pile load at the neutral plane (N_{max}) decrease considerably as the A_{rsp} increases, while the axial force at the pile base experiences only a slight reduction. It is also observed that the neutral plane shifts downward as the A_{rsp} ratio increases.

As illustrated in Fig. 10, N_{head} decreases by 14.8%, 17%, 25.2%, 41.7%, and 59.3% as A_{rsp} increases from 0% to 4.2%, from 0% to 6.5%, from 0% to 9.3%, from 0% to 16.7%, and from 0% to 26.1%, respectively. Meanwhile, N_{max} decreases by 4.3%, 6.9%, 10.8%, 17.8%, and 23.3% over the same A_{rsp} intervals.

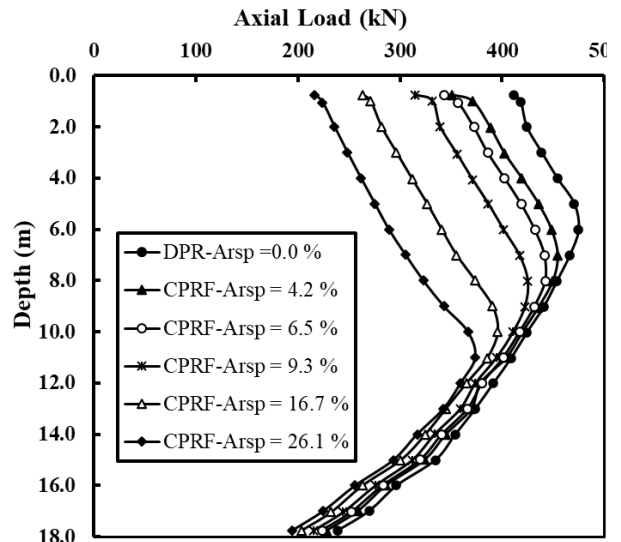


Fig. 9. Axial load distribution along the long pile near the raft center for different area ratios of short piles.

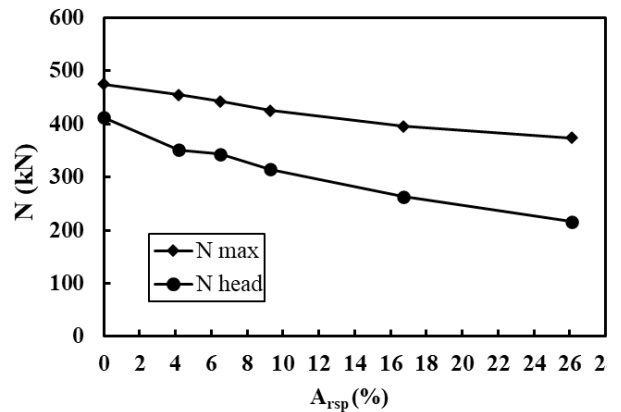


Fig. 10. Variation of N_{head} and N_{max} for the long pile near the raft center with the area ratio of short piles.

Based on the findings in this section, the short piles' area ratio (A_{rsp}) significantly affects the CPRF's behavior. A higher A_{rsp} enhances the performance of the shallow soft clay, leading to reduced raft settlement, an increased load supported by the short piles, and less load transferred to both the subsoil and long piles. The optimal A_{rsp} for minimizing CPRF settlement in the studied cases is 9.3%.

4.3. EFFECT OF THE LENGTH OF THE SHORT PILES ON CPRF

To study the impact of short pile length on the performance of CPRF, various lengths of short piles are considered. The short pile length (L_{sp}) is represented as a ratio of the thickness of the soft clay strata (H) beneath the raft, denoted as L_{sp}/H . The L_{sp}/H ratios considered in this study are 0.2, 0.3, 0.4, 0.5, 0.6, and 1.

4.3.1. SETTLEMENT OF THE RAFT

Fig. 11 presents the load-settlement curves of the CPRF for different L_{sp}/H ratios under a vertically distributed load of 100 kPa. For comparison, the load–settlement curve of the DPR ($L_{sp}/H = 0$) is also included. As depicted in Figure 11, as the L_{sp}/H ratio rises, the CPRF settlement reduces. This is because the increased pile length increases the contact surface area with the adjacent soil. Consequently, the pile load is distributed over a greater area of soil, reducing stress concentration in the soil and minimizing soil compression and settlement. This finding is in agreement with [22]. On the other hand, it is significant to note that for L_{sp}/H ratios of 0 and 0.2, the highest settlement surpasses the permissible values.

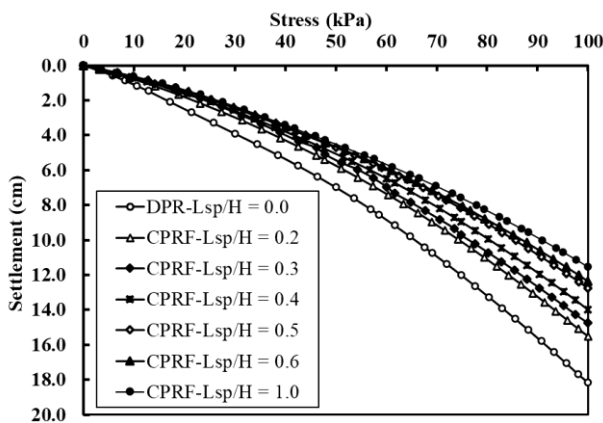


Fig. 11. Load-settlement curves for DPR and CPRF with different short pile lengths.

Fig. 12 illustrates the impact of the L_{sp}/H ratio on the SRF at a load level of 100 kPa, showing a decrease in the SRF as the L_{sp}/H ratio increases. A significant reduction in SRF (about 30%) occurs when the L_{sp}/H ratio increases from 0 to 0.5. However, for L_{sp}/H greater than 0.5, the SRF continues to decrease, but at a reduced rate, with only a 10% reduction as the L_{sp}/H increases from 0.5 to 1. Thus, it can be concluded that there exists an optimum L_{sp}/H ratio. In the studied cases, the optimum L_{sp}/H ratio is 0.5.

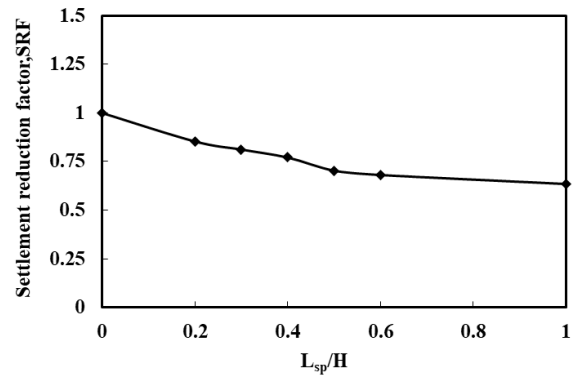


Fig. 12. Variation of settlement reduction factor with short pile length at a load level of 100 kPa.

4.3.2. LOAD SHARING BETWEEN PILES AND SUBSOIL

Fig. 13 depicts the impact of the L_{sp}/H ratio on the load distributed among long piles, short piles, and the subsoil. As the L_{sp}/H ratio increases, the short piles carry a larger portion of the load, while the load transferred to both the subsoil and the long piles slightly decreases. This limited rise in the short piles load results from an increase in the length of the short piles while keeping their diameter constant, which raises the slenderness ratio of the flexible piles, reducing their lateral stiffness and making them more prone to bulging under loads. This response aligns with the findings reported in [31].

Fig. 13 illustrates that, when L_{sp}/H exceeds 0.5, the additional load carried by the short piles is minimal and can be ignored. These results support the selection of an optimal L_{sp}/H ratio of 0.5 for the analyzed cases.

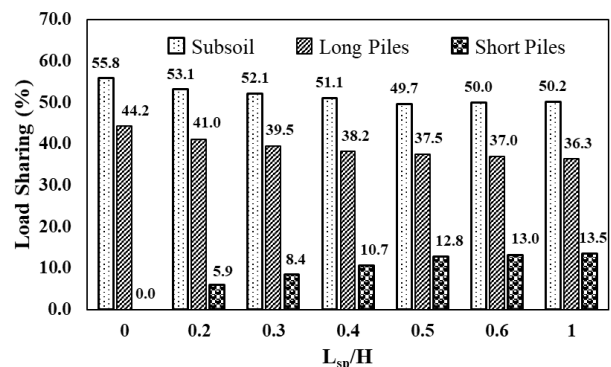


Fig. 13. Load sharing of CPRF for different short pile lengths at a load level of 100 kPa.

4.3.3. AXIAL LOAD ALONG THE LONG PILE

Fig. 14 presents the impact of the L_{sp}/H ratio on the distribution of the axial force across the long pile (near the raft center) in the CPRF. The results indicate that both the N_{head} and N_{max} decrease as the L_{sp}/H ratio increases; this behavior is consistent with the trends shown in Fig. 13. Additionally, as the L_{sp}/H ratio rises, the depth of the neutral plane beneath the pile head moves downward.

As shown in Fig. 15, N_{head} decreases by 11.5%, 16.17%, 21.04%, 23.4%, 24.03%, and 26.3% as the L_{sp}/H ratio increases from 0 to 0.2, from 0 to 0.3, from 0 to 0.4, from 0 to 0.5, from 0 to 0.6, from 0 to 1, respectively. Meanwhile, N_{max} decreased by 4.6%, 7.1%, 8.63%, 10.44%, 13.6% and 16.2% over the same L_{sp}/H ratio intervals. It is apparent that the impact of the short pile length on both N_{head} and N_{max} is less significant compared to the influence of the short pile’s area ratio.

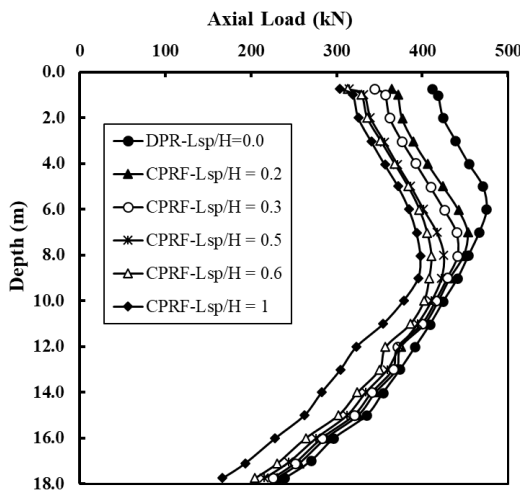


Fig. 14. Axial load distribution along the long pile near the raft center for different short pile lengths.

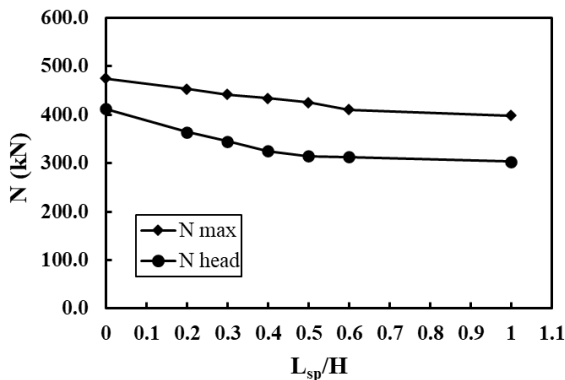


Fig. 15. Variation of N_{head} and N_{max} for the long pile near the raft center with short pile length.

The findings in this section demonstrate that

increasing the short pile length reduces CPRF settlement, increases the load carried by the short piles, and somewhat decreases the load transferred to both the long piles and the subsoil. Additionally, it is observed that the increase in short pile length has a greater impact on improving the settlement performance of the CPRF than on affecting the load sharing behavior. To achieve optimal performance of the CPRF systems analyzed, considering both settlement reduction and load supported by the short piles, a short pile with an L_{sp}/H ratio of 0.5 is advised.

4.4. EFFECT OF THE STIFFNESS OF THE SHORT PILES ON CPRF

Numerical analyses are performed to investigate the influence of short pile material stiffness on CPRF behavior, using common materials like coarse sand, stones, sandy gravel, and soil-cement. These materials have stiffness values ranging from 38 MPa to 320 MPa. The short pile stiffness (E_{sp}) is expressed as a ratio to the soil stiffness (E_s), with the E_{sp}/E_s ratios analyzed as 12.2, 22.4, 38.5, and 102.5.

4.4.1. SETTLEMENT OF THE RAFT

The load–settlement curves of the CPRF with different E_{sp}/E_s ratios subjected to uniform loading of 100 kPa are illustrated in Fig. 16. For reference, the load–settlement curve of the DPR ($E_{sp}/E_s = 0$) is additionally provided. The findings demonstrate that for all the considered CPRFs, the raft settlement is considerably decreased to an acceptable limit. Moreover, the settlement of the CPRF decreases as the E_{sp}/E_s ratio increases. This is because the higher stiffness of the short piles improves their load-carrying capacity, thereby enhancing the settlement performance of the CPRF. This is consistent with the findings presented in [23, 29].

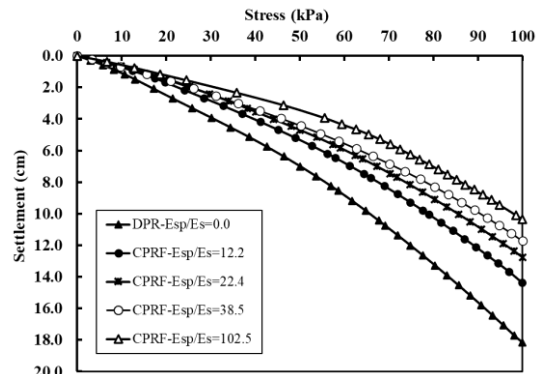


Fig. 16. Load-settlement curves for DPR and CPRF with different short pile stiffness.

Fig. 17 displays the impact of the E_{sp}/E_s ratio on the SRF at a load level of 100 kPa. It is apparent that when the E_{sp}/E_s ratio rises, the SRF reduces. The reduction in the SRF is significant as the stiffness of short piles increases up to an E_{sp}/E_s ratio of 38.5. After this point, the decrease in SRF becomes less pronounced. Therefore, it can be concluded that the optimum E_{sp}/E_s ratio for the examined cases is 38.5.

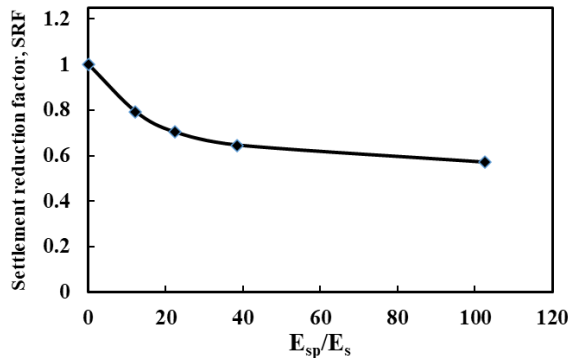


Fig. 17. Variation of settlement reduction factor with short pile stiffness at a load level of 100 kPa.

4.4.2. LOAD SHARING BETWEEN PILES AND SUBSOIL

Fig. 18 illustrates the influence of the E_{sp}/E_s ratios on the load distributed among the CPRF components. When the E_{sp}/E_s ratio rises, the short piles load significantly rises, whereas the load transferred to the subsoil and long piles diminishes. This occurs as strengthening the rigidity of the short piles helps relieve stress concentration on the long piles, which in turn decreases the load on the long piles while increasing the load carried on the short piles. This behavior aligns with the findings presented in [23].

As the E_{sp}/E_s ratio increases from 0 to 102.5, the short piles carry 30.8% of the entire load, while the load on the subsoil and the long piles decrease by 27.78% and 34.6%, respectively.

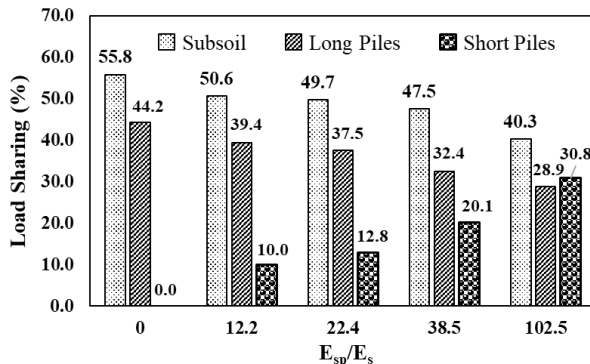


Fig. 18. Load sharing of CPRF for different short pile

stiffnesses at a load level of 100 kPa.

4.4.3. AXIAL LOAD ALONG THE LONG PILE

Fig. 19 demonstrates the impact of the E_{sp}/E_s ratios on the distribution of axial force within the long pile (near the raft center) within the CPRF. The results show that both the N_{head} and N_{max} decrease with the increase of the E_{sp}/E_s ratio. This behavior aligns with the trends observed in Fig. 18. Moreover, as the E_{sp}/E_s ratio increases, the neutral plane's depth beneath the pile head shifts downward.

As shown in Fig. 20, N_{head} decreases by 14.41%, 23.49%, 36.12%, and 49.19% as the E_{sp}/E_s ratio rises from 0 to 12.5, 0 to 22.4, 0 to 38.5, and 0 to 102.5, respectively. Meanwhile, N_{max} decreased by 5.63%, 10.44%, 16.7%, and 23.84% over the same E_{sp}/E_s ratio intervals. It is evident that the impact of the short pile stiffness on both N_{head} and N_{max} becomes less pronounced once the E_{sp}/E_s ratio surpasses 38.5.

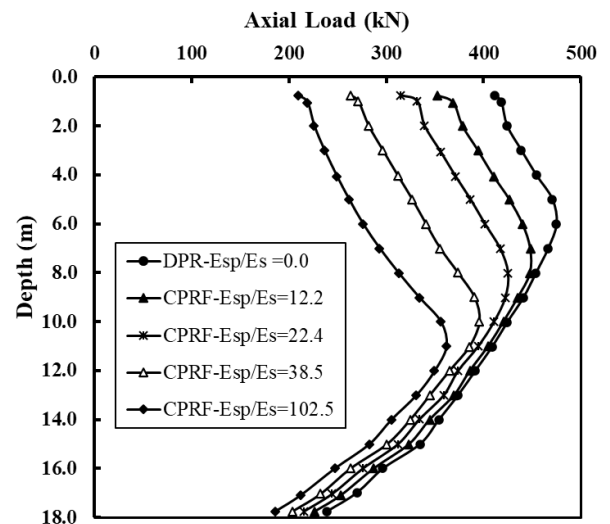


Fig. 19. Axial load distribution along the long pile near the raft center for different short pile stiffnesses.

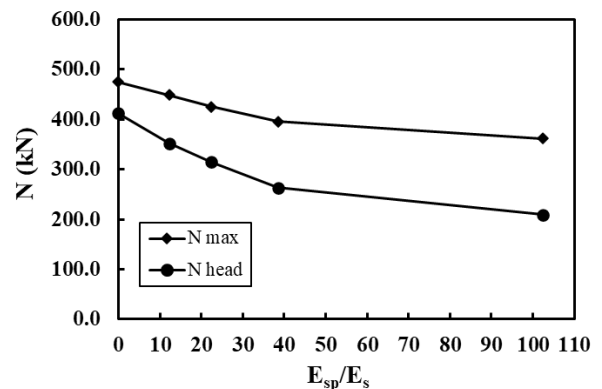


Fig. 20. Variation of N_{head} and N_{max} for the long pile near the raft center with short pile stiffness.

The results from this section indicate that the short pile stiffness (E_{sp}) has a substantial impact on CPRF's performance. As the E_{sp} increases, the settlement behavior of the CPRF gets better, the load transmitted to the short piles rises, and the load on both the long piles and the subsoil is reduced. For settlement reduction, the optimal E_{sp}/E_s ratio for the examined cases is 38.5.

4.5. EFFECT OF THE THICKNESS OF THE CUSHION ON CPRF

To examine the effect of the cushion thickness on CPRF performance, different thicknesses are analyzed, with the cushion thickness (t_c) varying between 0.25 and 1.50 m.

4.5.1. SETTLEMENT OF THE RAFT

Fig. 21 presents the load-settlement curves of the CPRF for varying cushion thicknesses under a vertically distributed load of 100 kPa. The results show that at the highest applied load, the raft's settlement is decreased to a tolerable limit for all the examined CPRFs. Additionally, the outcomes indicate that when the cushion thickness (t_c) rises, the settlement of the CPRF increases. This can be attributed to increasing the cushion thickness, which helps to reduce stress concentration on the long piles, which increases the load transferred to the subsoil, which in turn causes the settlement of the CPRF to increase. This is consistent with the findings presented in [20, 23].

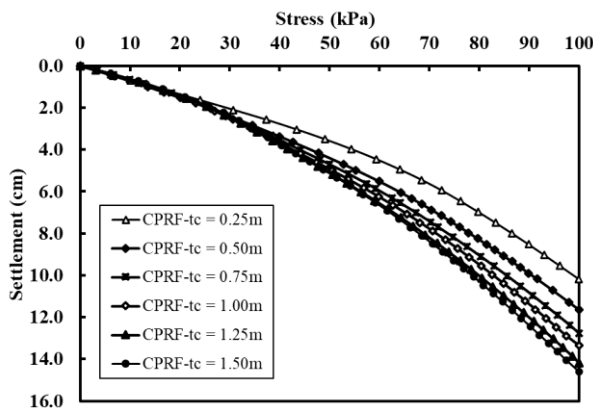


Fig. 21. Load-settlement curves for CPRF with different cushion thicknesses.

Fig. 22 illustrates the impact of the thickness of the cushion (t_c) on the maximum settlement of CPRF at a load level of 100 kPa. It is apparent that as t_c increases, the maximum settlement also increases. When t_c is increased from 0.25m to 0.75m, the maximum settlement increases by 25.4%. However,

when t_c further increased from 0.75m to 1.5m, the maximum settlement continued to increase, but at a relatively slower rate, with a 14.3% increase.

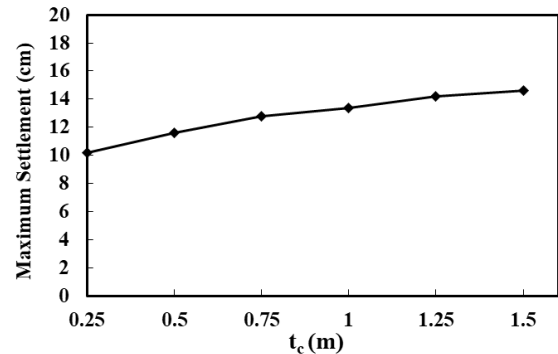


Fig. 22. Variation of maximum settlement with cushion thickness at a load level of 100 kPa.

4.5.2. LOAD SHARING BETWEEN PILES AND SUBSOIL

Fig. 23 depicts the impact of the cushion thickness on the load distributed among short piles, long piles, and subsoil under a load level of 100 kPa. As shown in Fig. 23, generally, when the cushion thickness (t_c) rises, the load transferred to both the subsoil and the short piles increases, while the load on the long piles decreases. This happens because increasing the cushion thickness helps alleviate stress concentration on the long piles, which reduces their load and increases the load transferred to the short piles and subsoil. This behavior agrees with the findings reported in [25].

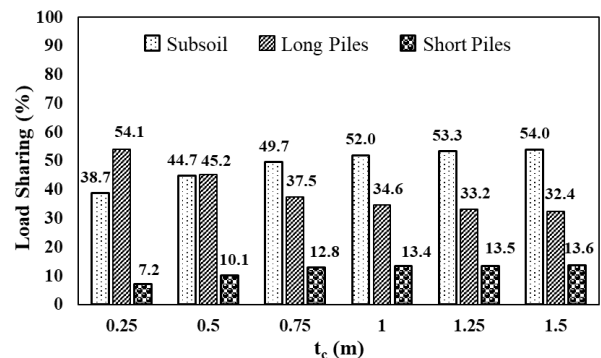


Fig. 23. Load sharing of CPRF for different cushion thicknesses at a load level of 100 kPa.

Fig. 23 demonstrates that as t_c increases from 0.25m to 0.75m, the load on the long piles decreases significantly by approximately 30.7%, while the load on the short piles and subsoil increases by 77.78% and 28.4%, respectively. However, once the cushion thickness exceeds 0.75m, the change in the load carried by the CPRF becomes less pronounced. That is, as t_c increases from 0.75m to 1.50m, the load on the

long piles decreases by 13.6 %, while the load on the short piles and subsoil increases by 6.25% and 8.65%, respectively. These results indicate that a cushion thickness of 0.75m is most effective for optimizing the bearing capacities of the short piles and subsoil in the analyzed cases.

4.5.3. AXIAL LOAD ALONG THE LONG PILE

The impact of the cushion thickness on the distribution of the axial force across long pile (near the raft center) within the CPRF is presented in Fig. 24. It is observed that both N_{head} and N_{max} diminish with increasing cushion thickness, following the same trend shown in Fig. 23. Additionally, irrespective of the cushion thickness, the pile base's axial force is almost constant at 215 kN. Also, as the cushion thickness increases, the neutral plane gradually shifts to a deeper level.

As illustrated in Fig. 25, N_{head} decreases by 10.53%, 18.25%, 22.04%, 24.45%, and 25.36% as t_c increases from 0.25m to 0.50m, 0.25m to 0.75m, 0.25m to 1.00m, 0.25m to 1.25m, and 0.25m to 1.50m, respectively. Meanwhile, N_{max} decreases by 8.54%, 9.61%, 8.88%, 9.33%, and 10.16% over the same t_c intervals.

The results from this section demonstrate that the cushion thickness significantly impacts the performance of the CPRF. With an increase in cushion thickness, the settlement of the CPRF rises, while the load on the short piles and subsoil increases and the load on the long piles reduces. The most effective cushion thickness for optimizing the bearing capacities of the short piles and subsoil in the studied cases is found to be 0.75m.

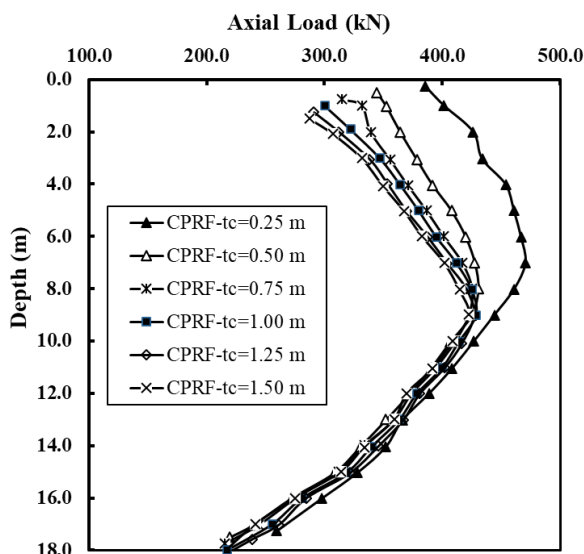


Fig. 24. Axial load distribution along the long pile near

the raft center for different cushion thicknesses.

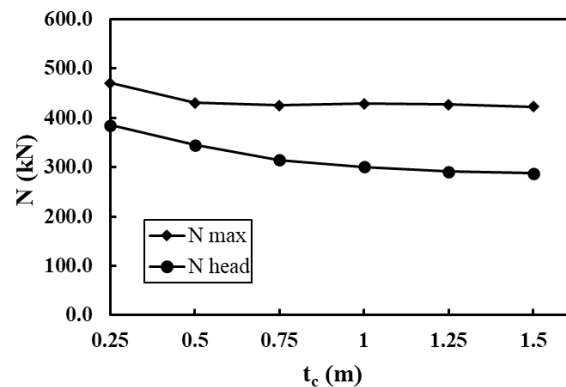


Fig. 25. Variation of N_{head} and N_{max} for the long pile near the raft center with cushion thickness.

4.6. EFFECT OF THE STIFFNESS OF THE CUSHION ON CPRF

To examine the influence of cushion material stiffness on CPRF behavior, numerical simulations are conducted using typical soil materials, including loose sand, medium sand, dense sand, and sandy gravel. The cushion stiffness (E_c) varies from 18 MPa to 120 MPa to represent the common range of soil materials used in practical applications.

4.6.1. SETTLEMENT OF THE RAFT

Fig. 26 illustrates the load-settlement curves of the CPRF for various cushion stiffnesses subjected to a uniform loading of 100 kPa. The results indicate that as E_c increases, the CPRF settlement decreases. This occurs because increasing the stiffness of the cushion increases stress concentration on the long piles, increasing their load and decreasing the load carried by both the short piles and the subsoil, thus reducing the CPRF's settlement. This aligns with the results in [23, 31]. Nevertheless, it should be mentioned that the highest settlement surpasses the acceptable values for the studied CPRF when the cushion's Young's modulus is 18 MPa and 30 MPa.

Fig. 27 illustrates the effect of cushion stiffness on the maximum settlement for the CPRF at a load level of 100 kPa. As illustrated in Fig. 27, the peak settlement of the CPRF decreases by 9.6%, 17%, and 16.76% as E_c increases from 18 MPa to 30 MPa, 30 MPa to 48 MPa, and 48 MPa to 120 MPa, respectively. The results indicate that dense sand (i.e., $E_c = 48$ MPa) is suggested as a more economical material for controlling settlements in the studied CPRFs.

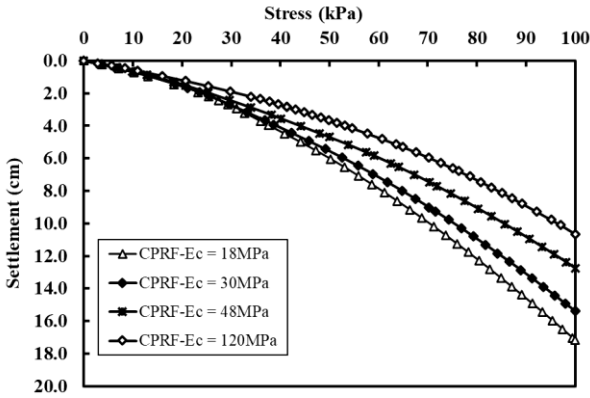


Fig. 26. Load-settlement curves for CPRF with different cushion stiffness.

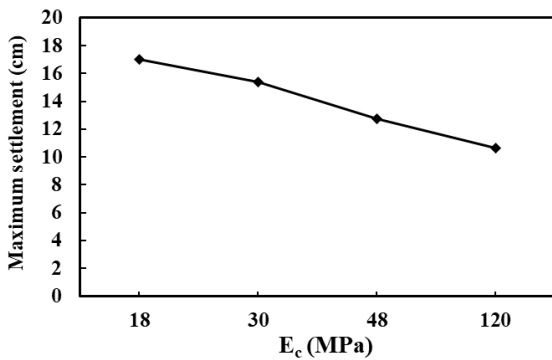


Fig. 27. Variation of maximum settlement with cushion stiffness at a load level of 100 kPa.

4.6.2. LOAD SHARING BETWEEN PILES AND SUBSOIL

Fig. 28 depicts the influence of cushion stiffness on the load distribution among CPRF components under a load level of 100 kPa. The findings reveal that as E_c rises, the load transmitted to short piles and the subsoil reduces, while the load borne by the long piles significantly increases. As an illustration, the long piles only support 20.3% of the entire imposed load, with a cushion having E_c of 18 MPa, while the subsoil and short piles bear 61.2% and 18.5%, respectively. On the other hand, with a higher cushion rigidity (i.e., E_c of 120 MPa), the short piles and subsoil share 42.1% and 11.6%, respectively, while the long piles bear 46.3% of the total load.

These findings suggest that a cushion stiffness of 48 MPa is the most efficient in optimizing the bearing capacities of the short piles and subsoil, while simultaneously keeping the settlement within allowable limits for the cases examined.

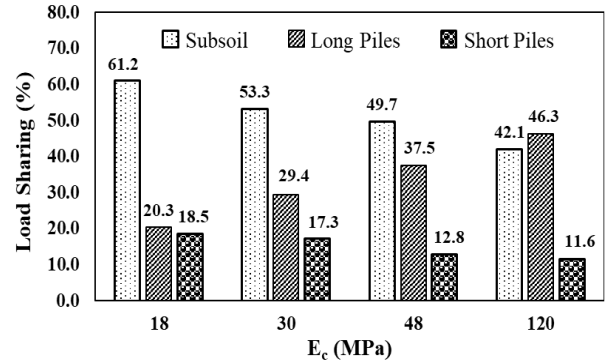


Fig. 28. Load sharing of CPRF for different cushion stiffnesses at a load level of 100 kPa.

4.6.3. AXIAL LOAD ALONG THE LONG PILE

Fig. 29 depicts how the cushion stiffness affects the axial force distribution along the long pile (near the raft center) in CPRF. It is evident that both N_{head} and N_{max} increase as the cushion stiffness increases, aligning with the trends observed in Fig. 28. Furthermore, as E_c increases, the neutral plane under the pile head gradually moves upward to a shallower depth.

As shown in Fig. 30, N_{head} increases by 50.8%, 32.2%, 31.6% as E_c rises from 18 MPa to 30 MPa, from 30 MPa to 48 MPa, and from 48 MPa to 120 MPa, respectively. Meanwhile, N_{max} increases by 12.86%, 9.21%, and 8.3% for the same E_c intervals.

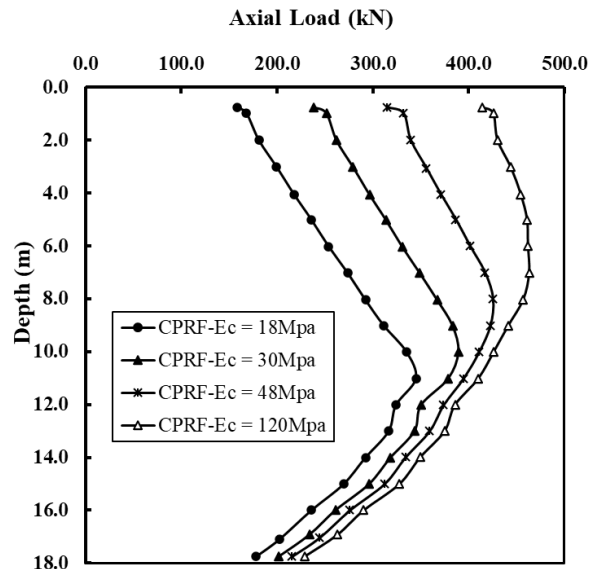


Fig. 29. Axial load distribution along the long pile near the raft center for different cushion stiffnesses.

The findings from this section reveal that the cushion stiffness significantly influences the behavior of the CPRF. As the stiffness of the cushion rises, the settlement of the CPRF decreases, with the load on the long piles increasing, and the load

transferred to the short piles and subsoil decreasing. A cushion with a stiffness of 48 MPa has been determined to be the most optimal for optimizing the bearing capacities of the subsoil and short piles, while ensuring that the settlement remains within permissible limits for the cases considered.

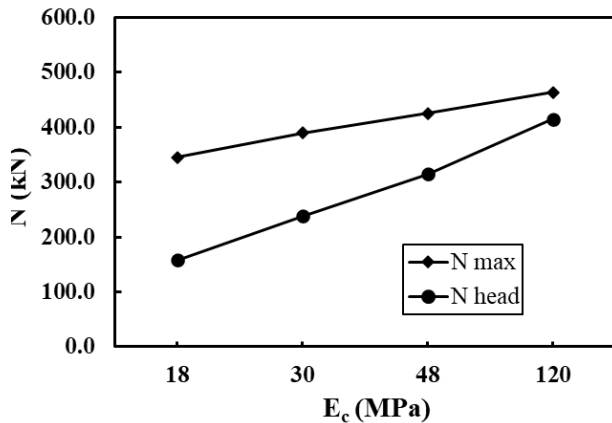


Fig. 30. Variation of N_{head} and N_{max} for the long pile near the raft center with cushion stiffness.

5. CONCLUSIONS

The 3D FE approach is used to conduct a detailed parametric study to examine the influence of several key factors on the performance of the uniformly loaded composite piled raft foundation (CPRF) on soft clay under drained conditions. The study examines the effects of the area replacement ratio, the length and stiffness of short piles, and the thickness and stiffness of the cushion on the settlement performance of the CPRF, the load transmitted by the long piles, short piles, and the subsoil, and the axial loads experienced by the end-bearing disconnected long piles. The key conclusions drawn from the parametric study are as follows:

1. The area ratio of the short piles (A_{rsp}) has a notable influence on the behavior of the CPRF. Increasing the A_{rsp} enhances the performance of the shallow soft clay, which reduces settlement of the raft, increases the load on the short piles, and decreases the load transferred to both the long piles and subsoil. The optimal A_{rsp} for reducing CPRF settlement for the studied cases is 9.3%.
2. Increasing the length of the short piles results in a reduction in CPRF settlement, a higher load carried by the short piles, and a slight reduction in the load carried by both the subsoil and the long piles. Additionally, it is noted that lengthening the short piles has a greater impact on improving the CPRF's

settlement performance than on affecting the load-sharing behavior. For the optimal performance of the analyzed CPRF systems, with respect to both settlement reduction and the load carried by the short piles, a short pile with an L_{sp}/H ratio of 0.5 is recommended.

3. The short piles' stiffness (E_{sp}) significantly influences the performance of the CPRF. A higher E_{sp} enhances the settlement characteristics of the CPRF, raises the load transmitted by the short piles, and reduces the load carried by the underlying soil and the long piles. For settlement reduction, the optimal E_{sp}/E_s ratio for the examined cases is 38.5.
4. The cushion thickness has a considerable impact on the behavior of the CPRF. With an increase in cushion thickness, the settlement of the CPRF rises, while the load on the long piles decreases, and more load is transmitted to the subsoil and short piles. A cushion thickness of 0.75m is found to be the most effective for optimizing the bearing capacities of the short piles and subsoil in the analyzed cases.
5. The stiffness of the cushion significantly affects the performance of the CPRF. Increasing the cushion stiffness results in a reduction in the CPRF settlement, while the long piles carry a greater load, and less load is transferred to the short piles and subsoil. A cushion stiffness of 48 MPa proves to be the most effective in optimizing the bearing capacities of the short piles and subsoil, while simultaneously keeping the settlement within acceptable limits for the analyzed cases.

REFERENCES

- [1] R. Banerjee, S. Bandyopadhyay, A. Sengupta, and G. R. Reddy, "Settlement behaviour of a pile raft subjected to vertical loadings in multilayered soil," *Geomech. Geoenjin.*, vol. 17, no. 1, pp. 282–296, 2022.
- [2] P. Halder and B. Manna, "Performance evaluation of piled rafts in sand based on load-sharing mechanism using finite element model," *Int. J. Geotech. Eng.*, vol. 16, no. 5, pp. 574–591, 2022.
- [3] O. A. Abdel-Azim, K. Abdel-Rahman, and Y. M. El-Mossallamy, "Numerical investigation of optimized piled raft foundation for high-rise building in Germany," *Innov. Infrastruct. Solut.*, vol. 5, pp. 1–11, 2020.

- [4] A. Z. Elwakil and W. R. Azzam, "Experimental and numerical study of piled raft system," *Alexandria Eng. J.*, vol. 55, no. 1, pp. 547–560, 2016.
- [5] A. M. Alnuaim, H. El Naggar, and M. H. El Naggar, "Evaluation of piled raft performance using a verified 3D nonlinear numerical model," *Geotech. Geol. Eng.*, vol. 35, pp. 1831–1845, 2017.
- [6] B. El-Garhy, A. A. Galil, A.-F. Youssef, and M. A. Raia, "Behavior of raft on settlement reducing piles: Experimental model study," *J. Rock Mech. Geotech. Eng.*, vol. 5, no. 5, pp. 389–399, 2013.
- [7] V. Fioravante, D. Giretti, and M. Jamiolkowski, "Physical modeling of raft on settlement reducing piles," in *From research to practice in geotechnical engineering*, 2008, pp. 206–229.
- [8] J. B. Burland, "' Piles as settlement reducers,' Invited Lecture," *XIX Convegno Ital. di Geotec.*, vol. 2, pp. 21–34, 1995.
- [9] X. D. Cao, I. H. Wong, and M.-F. Chang, "Behavior of model rafts resting on pile-reinforced sand," *J. Geotech. geoenvironmental Eng.*, vol. 130, no. 2, pp. 129–138, 2004.
- [10] A. Taghavi Ghalesari, A. Barari, P. Fardad Amini, and L. B. Ibsen, "Development of optimum design from static response of pile-raft interaction," *J. Mar. Sci. Technol.*, vol. 20, pp. 331–343, 2015.
- [11] I. H. Wong, M. F. Chang, and X. D. Cao, "17. Raft foundations with disconnected settlement-reducing piles," *Des. Appl. raft Found.*, vol. 10, 2000.
- [12] A. M. J. Alhassani and A. N. Aljorany, "Experimental and Numerical Modeling of Connected and Disconnected Piled Raft," *KSCE J. Civ. Eng.*, vol. 27, no. 6, pp. 2442–2454, 2023.
- [13] A. Saeedi Azizkandi, H. Rasouli, and M. H. Baziar, "Load sharing and carrying mechanism of piles in non-connected pile rafts using a numerical approach," *Int. J. Civ. Eng.*, vol. 17, pp. 793–808, 2019.
- [14] F. Tradigo, F. Pisanò, C. Di Prisco, and A. Mussi, "Non-linear soil-structure interaction in disconnected piled raft foundations," *Comput. Geotech.*, vol. 63, pp. 121–134, 2015.
- [15] A. Ata, E. Badrawi, and M. Nabil, "Numerical analysis of unconnected piled raft with cushion," *Ain Shams Eng. J.*, vol. 6, no. 2, pp. 421–428, 2015.
- [16] H.-J. Park et al., "Centrifuge modeling of disconnected piled raft using vertical pushover tests," *Acta Geotech.*, vol. 15, pp. 2637–2648, 2020.
- [17] M. El Sawwaf, "Experimental study of eccentrically loaded raft with connected and unconnected short piles," *J. Geotech. geoenvironmental Eng.*, vol. 136, no. 10, pp. 1394–1402, 2010.
- [18] P. Halder and B. Manna, "Load transfer mechanism for connected and disconnected piled raft: a comparative study," *Acta Geotech.*, vol. 17, no. 7, pp. 3033–3045, 2022.
- [19] P. Halder and B. Manna, "Large scale model testing to investigate the influence of granular cushion layer on the performance of disconnected piled raft system," *Acta Geotech.*, vol. 16, no. 5, pp. 1597–1614, 2021.
- [20] Ahmed M. Abdel Galil, Ahmed A. Elsobky, Abdel-Fattah A. Youssef, "NUMERICAL PARAMETRIC STUDY FOR OPTIMAL DESIGN OF DISCONNECTED PILED RAFT FOUNDATION," *J. Contemp. Technol. Appl. Eng.*, vol. 3, no. 2, pp. 63 – 81, 2025, doi: DOI: 10.21608/jctae.2025.360608.1042.
- [21] A. Ferchat, S. Benmebarek, and M. N. Houhou, "3D numerical analysis of piled raft interaction in drained soft clay conditions," *Arab. J. Geosci.*, vol. 14, pp. 1–12, 2021.
- [22] M. Samanta and R. Bhowmik, "3D numerical analysis of piled raft foundation in stone column improved soft soil," *Int. J. Geotech. Eng.*, vol. 13, no. 5, pp. 474–483, 2019.
- [23] F.-Y. Liang, L.-Z. Chen, and X.-G. Shi, "Numerical analysis of composite piled raft with cushion subjected to vertical load," *Comput. Geotech.*, vol. 30, no. 6, pp. 443–453, 2003.
- [24] M.-h. Zhao, L. Zhang, and M.-h. Yang, "Settlement calculation for long-short composite piled raft foundation," *Journal of Central South University of Technology*, vol. 13, no. 6, pp. 749–754, 2006.
- [25] J.-J. Zheng, S. W. Abusharar, and X.-Z. Wang, "Three-dimensional nonlinear finite element modeling of composite foundation formed by CFG-lime piles," *Comput. Geotech.*, vol. 35, no. 4, pp. 637–643, 2008.

- [26] X. Wang, J. Zheng, and J. Yin, "On composite foundation with different vertical reinforcing elements under vertical loading: a physical model testing study," *J. Zhejiang Univ. Sci. A*, vol. 11, no. 2, pp. 80–87, 2010.
- [27] A. Eslami and S. S. Malekshah, "Analysis of non-connected piled raft foundations (NCPRF) with cushion by finite element method," *Comput. Methods Civ. Eng.*, vol. 2, no. 2, 2011.
- [28] R. Z. Moayed, E. Izadi, and M. Mirsepahi, "3D finite elements analysis of vertically loaded composite piled raft," *J. Cent. South Univ.*, vol. 20, pp. 1713–1723, 2013.
- [29] V. J. Sharma, S. A. Vasanvala, and C. H. Solanki, "Behaviour of load-bearing components of a cushioned composite piled raft foundation under axial loading," *Slovak J. Civ. Eng.*, vol. 22, no. 4, pp. 25–34, 2014.
- [30] W. El Kamash, H. El Naggar, M. Nabil, and A. Ata, "Optimizing the unconnected piled raft foundation for soft clay soils: numerical study," *KSCE J. Civ. Eng.*, vol. 24, no. 4, pp. 1095–1102, 2020.
- [31] B. M. El-Garhy, "A simplified method for the nonlinear analysis of composite piled raft foundation," *Geotech. Geol. Eng.*, vol. 40, no. 9, pp. 4357–4375, 2022.
- [32] R. Brinkgreve and P. A. Vermeer, "PLAXIS 3D reference manual CONNECT edition V20," Delft Univ. Delft, Netherlands, 2019.
- [33] M. H. Zakaria and A. Basha, "Two-Dimensional Numerical Approaches of Excavation Support Systems: A Comprehensive Review of Key Considerations and Modelling Techniques," *J. Contemp. Technol. Appl. Eng.*, vol. 3, no. 1, pp. 64–74, 2024.
- [34] F. M. El-Nahhas, A. Abdel-Rahman, M. Mansour, and O. Hamed, "Investigating the Behavior of an Existing Quay Wall Using the Characteristic Parameters of Port-Said Clay, Egypt 2017," *World Appl. Sci. J.*, vol. 35, no. 3, pp. 483–499, 2017.
- [35] R. B. J. Brinkgreve, E. Engin, and H. K. Engin, "Validation of empirical formulas to derive model parameters for sands," *Numer. methods Geotech. Eng.*, vol. 137, p. 142, 2010.
- [36] M. M. Killeen and B. McCabe, "A numerical study of factors affecting the performance of stone columns supporting rigid footings on soft clay," in *7th European Conference on Numerical Methods in Geotechnical Engineering*, Taylor and Francis, 2010.
- [37] Egyptian code for soil mechanics-design and construction of foundations, ECP-202, Sixth Ed., Part 3: Shallow Foundations, National Housing and Building Research Center, Cairo, 2001.